# Analysis and Development of a refined navigation algorithm for XNav mission

A project report submitted

in partial fulfillment for the award of the degree of

**Bachelor of Technology**

in

**Electronics and Communications Engineering**

by

**Karun Mathews Manoj**


**Department of Avionics**

**Indian Institute of Space Science and Technology**

**Thiruvananthapuram, India**

**May 2023**

# Certificate

This is to certify that the project report titled ***Analysis and Development of a refined navigation algorithm for XNav mission*** submitted by **Karun Mathews Manoj**, to the Indian Institute of Space Science and Technology, Thiruvananthapuram, in partial fulfillment for the award of the degree of **Bachelor of Technology** is a bona fide record of the original work carried out by him under my supervision. The contents of this project report, in full or in parts, have not been submitted to any other Institute or University for the award of any degree or diploma.

Dr. Priyadarshnam Hari
Professor

Name of Department Head
Designation

**Place:** Thiruvananthapuram
**Date:** May 2023

# Declaration

I declare that this project report titled ***Analysis and Development of a refined navigation algorithm for XNav mission*** submitted in partial fulfillment for the award of the degree of **Bachelor of Technology** in **Electronics and Communications Engineering** is a record of the original work carried out by me under the supervision of **Dr. Priyadarshnam Hari**, and has not formed the basis for the award of any degree, diploma, associateship, fellowship, or other titles in this or any other Institution or University of higher learning. In keeping with the ethical practice in reporting scientific information, due acknowledgments have been made wherever the findings of others have been cited.

**Place:** Thiruvananthapuram
**Date:** May 2023

Karun Mathews Manoj
(SC19B120)

*This project report is dedicated to my fellow students*

# Acknowledgements

I am grateful to Dr. Priyadarshnam for giving the opporunity to work on this project.

Karun Mathews Manoj

# Abstract

X-ray pulsar based navigation is a possible breakthrough technology which can provide a more reliable and independent means of navigation for deep space missions. In this work the existing X-ray pulsar based navigation algorithms for the XNav mission are reviewed and possible optimizations and modifications to the algorithm are developed. The CC and NLS estimators have been adapted for frequency estimation. Two new estimators - coarse frequency estimator and Maximum Likelyhood Estimator have been developed. So far, in this work 4 phase estimators have been tested for the case of a stationary spacecraft. Additionally a 1D kalman filter is used to smoothen the response from these estimators. The parameters for the simulation such as source and background intensity, bin size and observation time were taken referring to the literature. A new photon TOA generation algorithm has been developed based on the phase of arrival concept. 3D-LEO simulations have been performed, and true anomaly estimation results are shown.

# Contents

**List of Figures** viii

**List of Tables** ix

**Abbreviations** x

**1 Introduction** 1

1.1 Working Principle . . . . . 3
1.2 Literature review . . . . . 4
1.3 Motivation . . . . . 5
1.4 Objectives and Contributions . . . . . 5

**2 Methodology** 6

2.1 Simulation of Non Homogeneous Poisson Process by thinning . . . . . 7
2.2 Transformation of times to spacecraft reference point . . . . . 7
2.3 Division of TOAs into segments . . . . . 9
2.4 Coarse frequency estimation . . . . . 10
2.5 Average Shifted Histogram for epoch folding . . . . . 10
2.6 MLE estimator . . . . . 11
2.7 Continuous processing instead of Batch processing . . . . . 11
2.8 Kalman filtering the output of the estimators . . . . . 12

**3 Results and Discussion** 13

3.1 Testing the 4 phase estimators . . . . . 14
3.2 Performance of doppler and phase estimators in current scheme . . . . . 22
3.3 3D orbit simulation . . . . . 23

**4 Conclusion** **28**
4.1 Summary . . . . . 28
4.2 Contribution of the work . . . . . 28
4.3 Future work . . . . . 29

**Bibliography** **29**

**Appendices** **32**

**A True Anomaly estimation** **32**

# List of Figures


1.1 Navigation using X-ray Pulsars system block diagram . . . . . 3

2.1 observed frequency and phase shift over one orbit . . . . . 9

3.1 Crab pulsar pulse profiles . . . . . 13
3.2 Phase shift estimate vs time (Crab pulsar) . . . . . 15
3.3 Kalman filtered phase shift estimates (Crab pulsar) . . . . . 16
3.4 PSR B1509 pulse profiles . . . . . 17
3.5 Phase shift estimate vs time (PSR B1509) . . . . . 18
3.6 Kalman filtered phase shift estimates (PSR B1509) . . . . . 19
3.7 weak Crab pulsar pulse profiles . . . . . 20
3.8 Phase shift estimate vs time (weak Crab pulsar) . . . . . 21
3.9 Kalman filtered phase shift estimates (weak Crab pulsar) . . . . . 22
3.10 orbital parameters . . . . . 23
3.11 CC estimator . . . . . 24
3.12 MLE estimator . . . . . 24
3.13 True anomaly estimated . . . . . 25
3.14 True anomaly filtered . . . . . 26
3.15 CC estimate of radial velocity with FIR filtering . . . . . 27
3.16 True anomaly filtered . . . . . 27

# List of Tables

3.1 Performance of estimators in current scheme . . . . . 23

# Abbreviations

| | |
|---|---|
| $c$ | speed of light |
| $TOA$ | Time Of Arrival |
| $P$ | Period of pulsar |
| $f_s$ | pulsar source frequency |
| $w$ | angular velocity of orbiting satellite |
| $ECI$ | Earth-centered inertial coordinate frame |
| $n$ | Direction of pulsar in ECI frame, pulsar: $B0531 + 21$ |
| $N_b$ | Number of bins |
| $T_{obs}$ | Observation Time |
| $CC$ | Cross Correlation |
| $FFT$ | Fast Fourier Transform |
| $GPS$ | Global Positioning System |
| $IMU$ | Inertial Measurement Unit |
| $MLE$ | Maximum Likelyhood Estimator |
| $NLS$ | Non linear least squares |
| $KG$ | Kalman Gain |
| $est$ | estimate |
| $mea$ | measurement |

# Chapter 1
# Introduction

The XNav mission is a proof of concept mission to demonstrate xray pulsar navigation as a possible means of navigation in deep space. Current methods of satellite navigation for extra-terrestrial missions use the Deep Space Network (DSN). With a combination of techniques such as Doppler ranging, Two way ranging, Delta-Differential One way ranging - the position and velocity of the spacecraft can be estimated reasonably.

However, as the spacecraft travels further away both it and the DSN have to deal with severe attenuation and propagation effects of the ranging signal. Morever, the rate at which it's state can be updated is limited by the time lag between it and the DSN back on earth. Thus development of a more independent means of navigation is beneficial.

The basic principle of xnav is to estimate the state (position and velocity), using the doppler shift and phase shift estimates. The doppler shift estimate gives an estimate of the radial velocity w.r.t the pulsar. The phase shift estimate gives an estimate of the time delay between the spacecraft and a reference point - from which relative distance between the spacecraft and the reference point can be calculated, along the pulsar direction.

This is done by capturing the pulsed emissions in the X-ray spectrum from suitable pulsars. These emissions are observed by an array of X-ray detectors. From these observations and using certain processing schemes the individual photon time of arrivals (TOAs) are obtained and recorded. Both the doppler and phase estimators take the TOAs as the raw data-from which the parameters (frequency and phase) are estimated.

The X-ray Pulsar Navigation System can be used in two ways. One way being that of a complementary navigation aid along with GPS and IMU. In this case, observing a single

pulsar is enough to improve navigation accuracy. Using multiple pulsar observations can further improve the level of accuracy.

It can also be used as an independent and autonomous navigation system - without GPS or any other external navigation aid. In this case however, at least 3 different pulsar observations have to be taken in order to estimate the complete state of the spacecraft. The 3 pulsars have to be selected so that they lie along non co-planar directions.

It is not necessary for the 3 pulsar observations to be taken simultaneously. They can be observed in an alternating fashion. In such an observation scheme, measurements for the two pulsars not being observed can be predicted using a model of the spacecraft motion. A proper scheduling for pulsar observations has to be maintained - so that observation time can be balanced between all the observed pulsars.

The block diagram for the Navigation using X-ray Pulsars system is shown in figure 1.1. This is how the final XNav framework is envisioned. Photons in the X-ray spectrum are captured by the detector array, and their times of arrival (TOAs) are recorded (it is important that in a set of observations, that all the photons observed are only from one pulsar). Then, based on a rough estimate of the trajectory (specifically, the radial velocity along the pulsar direction), the TOAs are divided into segments in which observed frequency is approximately constant ($\Delta f < 10^{-5} Hz$).

The MLE and CC estimators require a small frequency range to efficiently produce a frequency estimate. For this purpose, the Coarse Doppler Estimator is used. In here, the TOAs are binned and a time series (which corresponds to arrival rate) is obtained. The spectrum of the time series is obtained using the FFT. The "coarse frequency estimate" is then obtained by finding the peak in the spectrum in a range centered at the pulsar frequency (which would be observed at a stationary reference point).

Now either the MLE estimator or CC estimator can be used to get the final frequency and phase shift estimates. Both estimators have pros and cons- the CC estimator is seen to be the more reliable, but the MLE estimator can sometimes be more accurate, since it's optimum finding method doesn't have any fixed step size.

The time delay estimate is obtained by dividing the phase shift estimate by the frequency

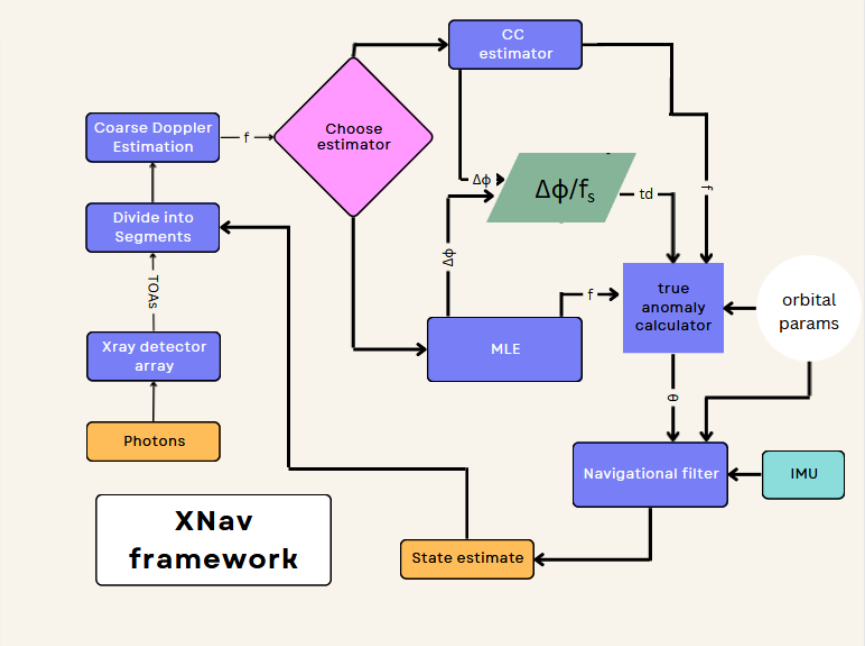


**Figure 1.1:** Navigation using X-ray Pulsars system block diagram

estimate.

Using time delay, observed frequency and expected orbital parameters- true anomaly of the spacecraft can be calculated [A]. From this, the position and velocity estimates can be calculated. The final estimates are obtained by filtering these estimates with the acceleration and rotation measurements from the IMU. The Unscented Kalman Filter was used previously for the purpose [1].

## 1.1 Working Principle

The two measurements provided by an X-ray Pulsar Navigation System are the doppler shift and phase shift. These correspond to the radial velocity $(v \cdot n)$ and radial position $(x \cdot n)$, respectively. The assumptions behind the estimation process are detailed in the methodology section.

The basic framework of this x-ray navigation system is as follows:

1. Detection of photon Time Of Arrivals (TOAs).
2. Division of TOAs into time segments in which the assumption

$|\hat{\dot{\phi}}(t_a) - \hat{\dot{\phi}}(t_b)| < 10^{-5} Hz$ holds, for a time segment $[t_a, t_b]$.

3. Coarse Estimation of observed pulsar frequency for individual segments.
4. Estimation of pulsar frequency (refined estimate) and phase shift, using either MLE or CC Estimators.
5. Time delay calculation.
6. True anomaly calculation using known satellite orbital parameters.
7. Position and Velocity state calculation and subsequent filtering using Unscented Kalman Filter (UKF).

## 1.2 Literature review

Much work has been previously done in this area. In 2005, Suneel Sheikh from the University of Maryland wrote a phd thesis [2] on this topic. The thesis contributes to a lot of knowledge in this domain. It contains a catalogue of different pulsars, and develops a suitable selection criterion for which pulsar to observe.

In 2020, Aashka Oza from IIST put forth a BTech project report on the topic, where cleaning of the observed pulsar data was discussed and a design for the small sat was shown.[3]

In 2021, Shreya Mishra from IIST also put forth a BTech project report which presents an extensive study of the detector and signal processing system. A method to calculate true anomaly from the time delay measurement was also shown.[4]

In the same year, Kandala et al. published a paper detailing the mission concept for a technology demonstration mission carried out in lower-earth orbit. Also further details about the instrumentation and system design were shown.[5]

In 2022, Shaurya Shrivastava from IIT Kharagpur put forth a master's thesis on this topic, which provided many contributions to this area. In his work, the performance of the estimators were tested and the Phase of Arrival (POA) formulation was incorporated into the simulations. 2d and 3d orbital simulations were also performed to study the performance of the estimators and understand the effect of bin size and observation time.[1]

There is also a paper published in 2020 by Su et al. [6] - this paper details the phase of arrival formulation which removes the need to perform time transformations on all the times of arrival (TOAs) detected at the spacecraft.

The papers from the SEXTANT (Station Explorer for X-ray Timing and Navigation Technology) mission by NASA, were also found to be very resourceful. Particularly, the pulse phase and doppler estimation algorithms are discussed in detail. The filter measurement model is also discussed. [7] [8] [9] [10]

## 1.3 Motivation

To design an autonomous navigation system based on X-ray pulsar navigation.

## 1.4 Objectives and Contributions

1. Resolve the problem of estimating the state of an accelerating spacecraft.
2. Add the velocity estimation capability.
3. Optimizing the estimation algorithms.
4. Addition of new filters to reduce noise.
5. Development of proper criteria for selection of bin size in epoch folding algorithm.

# Chapter 2
# Methodology

For a spacecraft moving in space, the observed pulsar signal will be distorted due to doppler effects. Also the photon times of arrival will be shifted due to relativistic effects and also gravitational effects of the surrounding bodies.

However if we consider the barycentre of our solar system, generally all such effects can be ignored. The Solar System Barycentre (SSB) can be considered a relatively stationary point with respect to the pulsar. Hence, we estimate a "true rate function" at this point in space. The empirical rate function which is to be estimated from our observations of the pulsar will be compared with the true rate function in order to estimate the relative phase shift.

To facilitate the development of the overall navigation algorithm, an accurate photon TOA generation algorithm needs to be present. In the absence of physical methods of simulating the photon arrival process from the pulsar, this is used. In this simulation, first the arrivals are simulated at the SSB. Then using the Phase of arrival (POA) formulation [6], we obtain the photon times of arrival at the spacecraft.

Although the code for this simulation has been developed previously, as well as some phase delay estimators which can be used on the generated times of arrival (TOAs)- getting consistent results for the phase estimate was found to be difficult. So a seperate piece of code has been developed which considers a simpler case of a stationary spacecraft, at which the pulsar signal has only a relative phase shift (caused by geometric time delay) with respect to the reference pulsar profile at the SSB.

Furthermore some important changes and additions have been made. These are detailed

below.

## 2.1 Simulation of Non Homogeneous Poisson Process by thinning

The arrival of photons from a weak source (such as a pulsar) can be modelled as a non homogeneous poisson process.

There are several methods of simulating the Non Homogeneous Poisson Process. One very efficient method which has not been found to be used in other x-ray pulsar navigation literature, is the method of thinning [11]. This method involves controlled deletion of arrivals from a set of homogeneous Poisson arrivals.

**Algorithm 2.1:** Algorithm to simulate NHPP by thinning

$x \leftarrow X \sim Pois(\lambda_{max} T_{obs})$;
$ts \leftarrow zeros(x)$;
$t_{thin} \leftarrow []$;
$count \leftarrow 0$;
**while** $count \leq x - 1$ **do**
  $ts[count] \leftarrow t \sim U(0, T_{obs})$;
  $p \leftarrow P \sim U(0, 1)$;
  **if** $p \leq \frac{\lambda(ts[count])}{\lambda_{max}}$ **then**
    $ts[count] \gg t_{thin}$;
  **end**
  $count \leftarrow count + 1$;
**end**
$sort(t_{thin})$;

## 2.2 Transformation of times to spacecraft reference point

An orbiting spacecraft is constantly in motion. Both position and velocity components along the pulsar direction are continuously varying. So the phase evolution of the pulse signal it observes, is quite different from that at a reference point. The two reasons for the difference in the phase evolution trajectory at the spacecraft and at the reference point are as

follows. Firstly, - there is an initial phase delay ($\phi_0$), at time $t_0$, coming from the radial displacement (along the pulsar direction) between spacecraft and reference point. Secondly, there is a doppler shift in the observed pulsar frequency ($f(\tau) \neq f_s$). In this work, the geocentre is taken as the reference point, and from now on use of the term reference point can be assumed to mean geocentre.

Phase evolution at the reference point and spacecraft can be written as follows:

$$\phi_{ref} = f_s t \tag{2.1}$$

$$\phi_{sc} = \phi_0 + \int_{t0}^{t} f(\tau) d\tau \tag{2.2}$$

A doubt may arise that- since the spacecraft is moving- doesn't the radial displacement change constantly, and so also the phase delay term? So should $\phi_0$ be changed as well? This is not necessary, as it is seen from the orbital simulations and curvefitted equations (2.4,2.5), that the change in phase delay is accounted for by change in frequency.

In order to transform arrival times at the reference observatory (geocentre) to arrival times seen at the spacecraft - the phase of arrival concept is used. The essential idea can be stated thus - " Phase at the spacecraft and at the reference observatory are exactly the same, only time at which this phase is seen is different." So essentially we have to solve for $t$ in the following equation:

$$f_s t_{ref} = \phi_0 + \int_{t0}^{t} f(\tau) d\tau \tag{2.3}$$

For the case of an orbiting satellite, it was found that $f_{sc}(t)$ can be well approximated by a sinusoidal function- which is easy to integrate. Thus the integral in (2.3) can also be obtained as a simple function of $t_{sc}$. With this function, we obtain an approximate expression for $\phi_{sc}$ (phase at spacecraft). From this we get an expression for $\Delta\phi(t)$ (phase bw spacecraft and reference point), which is simply $\phi_{sc} - f_s t$.

For an orbital simulation, position and velocity of a spacecraft are completely known, from this the trajectory of $f_{sc}(t)$ and $\Delta\phi(t)$ can be obtained. These two trajectories were calculated for a particular circular orbit, and they are shown below.

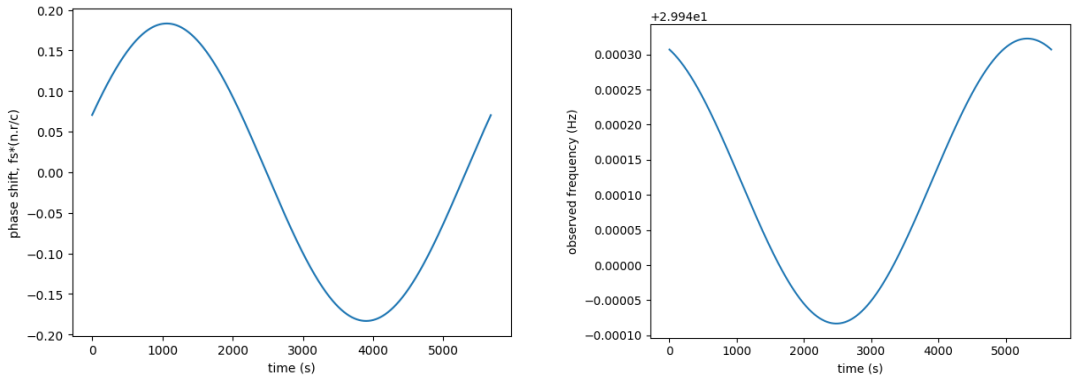


**Figure 2.1:** observed frequency and phase shift over one orbit- $fsc(t) = fs(1 + \frac{n \cdot v(t)}{c})$ and $\Delta\phi(t) = fs\frac{n \cdot r(t)}{c}$ are plotted over a 500km altitude LEO orbit.

Using these data points we fit $f_{sc}(t)$ and $\Delta\phi(t)$ (observed frequency and observed phase shift on spacecraft), according to the following model:

$$f_{sc}(t) = f_{mean} + Acos(wt + \psi_0) \tag{2.4}$$

$$\Delta\phi(t) = f_{mean}t + \frac{A}{w}sin(wt + \psi_0) + f_s\left(\frac{n \cdot r_0}{c}\right) - \frac{A}{w}sin(\psi_0) - f_s t \tag{2.5}$$

where, $f_{mean}$, $A$ and $\psi_0$ are the parameters being fitted. $r_0$ is the initial position of the spacecraft (at the simulation start time).

Once we have $f_{mean}$, $A$ and $\psi_0$ - we can obtain the transformed arrival time ($t_{sc}$) by solving the below equation for $t_{sc}$, given $t_{geo}$:

$$f_{mean}t_{sc} + \frac{A}{w}sin(wt_{sc} + \psi_0) + f_s\left(\frac{n \cdot r_0}{c}\right) - \frac{A}{w}sin(\psi_0) = f_s t_{geo} \tag{2.6}$$

Curve-fitting and solving the time transformation equation was done using the scipy.optimize package ([12]).

## 2.3 Division of TOAs into segments

We divide the observations over one orbit into 'segments'. In each segment, the change in observed pulsar frequency is less than $10^{-5}$ **Hz**. This condition is kept for the following

reason. For the pulsar selected in this work (crab pulsar), it was seen that changes in radial velocity of 0.5 **km/s** would change the observed frequency by $5 * 10^{-5}$ **Hz**.

So, if radial velocity were to change by such a magnitude, the peak in the frequency domain would be smeared over a range of $5*10^{-5}$ **Hz** and our velocity estimate would atleast have an error of 0.5 **km/s** (regardless of the estimator's performance). Restricting the segment length, reduces this kind of error.

## 2.4 Coarse frequency estimation

The frequencies of millisecond pulsars are kind of low compared to the frequencies used in doppler radar or radar guns (which also work based on doppler shift), and the doppler shift due to the motion of the observer is quite low.

For example: for a change in radial velocity $\Delta v_r$ = 0.5 **km/s**, doppler shift seen in crab pulsar frequency is $\Delta f = 4.99 * 10^{-5}$ **Hz**. For this reason, we require high frequency resolution in the spectrum generated using the FFT. To do this windowing (using 150 point rectangular window) and zero padding (to increase observation time by 9900 seconds (adding only zeros as new data)) are done.

The coarse frequency estimate is obtained by looking for the highest amplitude frequency component in the expected frequency variation range.

## 2.5 Average Shifted Histogram for epoch folding

A modification made to improve the performance of the phase estimators is binning of the arrival times using an average shifted histogram (ASH). The ASH is used to remove the effect of choice of bin origin. In the view of Scott (2009) [13], the choice of bin origin of a histogram is a nuissance parameter. The ASH averages the histogram over 'n' possible bin origins.

The ASH is also used to visualize the performance of the doppler and phase estimators.

## 2.6 MLE estimator

A Maximum Likelyhood Estimator has been developed, and it's phase estimation capabilities have been compared with that of the other estimators. A main difference between the MLE estimator from the others, is that it directly uses the times of arrival (TOAs) as measurements and does not perform epoch folding.

**Algorithm 2.2:** Algorithm for maximum likelyhood estimation

```
1  φ ← linspace(0, 1, 100);
2  t_thin ← [...] ;          /* This is the set of arrival times */
3  i ← 0;
4  φ̂ ← 0;
5  while i ≤ length(φ) do
6  |  j ← 0;
7  |  LLF ← 0;
8  |  while j ≤ length(t_thin) do
9  |  |  LLF ← LLF + log_2(λ(t_thin[j]; φ[i]));
10 |  |  j ← j + 1;
11 |  end
12 |  if i == 0 then
13 |  |  LLF_max ← LLF;
14 |  else
15 |  |  if LLF > LLF_max then
16 |  |  |  LLF_max ← LLF;
17 |  |  |  φ̂ ← φ[i];
18 |  |  end
19 |  end
20 |  i ← i + 1;
21 end
```

## 2.7 Continuous processing instead of Batch processing

All the estimators have been modified to allow continuous estimation of the phase- instead of producing a phase estimate only after the entire observation period is over. Every time a new photon arrival is detected, the sequence of arrival times with the new arrival time appended can be fed into the estimator- thus producing a new estimate.

Here also there are some inefficiencies - if every time we get a new arrival, we have to

reprocess the old arrivals as well - a lot of the old calculations are being repeated. For example, when calculating the empirical rate function, only the value in the bin corresponding to the new arrival actually changes, so there is no need to recalculate the value in the other bins.

In the MLE estimator as well, the new log likelyhood function value is simply the old value added to a contribution by the new arrival. So, the old value should be reused.

This also has to be tested on the hardware. If the rate of arrivals is quite high, the estimate from one arrival may not be completely processed by the time the next arrival happens. In that case, some form of batch processing has to be used. So that an estimate is generated only only after the previous set of arrivals has been processed.

## 2.8 Kalman filtering the output of the estimators

1D Kalman filtering has been used to smoothen the phase estimate obtained from the phase estimators. It has been implemented using the continuous processing idea.

**Algorithm 2.3:** Kalman filtering of phase estimate

```
1  toa = [...] ;            /* This is the set of arrival times */
2  t_thin ← [];
3  i ← 0;
4  E_EST ← [0.5];
5  EST ← [0.2];
6  E_MEA ← 0.5 ;                          /* this remains fixed */
7  while i < length(toa) do
8  |  toa[i] ≫ t_thin ;          /* new arrival times are appended */
9  |  MEA ← estimator(t_thin);
10 |  KG ← E_EST[i] / (E_MEA + E_EST[i]);
11 |  EST[i] + KG * (MEA − EST[i]) ≫ EST;
12 |  (1 − KG) * E_EST[i] ≫ E_EST;
13 |  i ← i + 1;
14 end
```

Note: $estimator(t_{thin})$ is the estimated phase given by a particular estimator.

# Chapter 3

# Results and Discussion

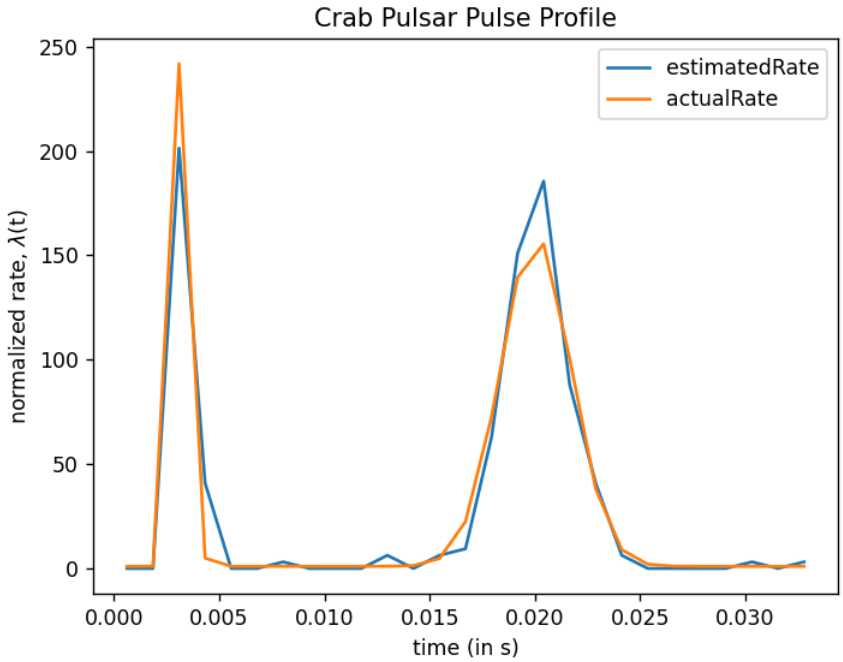


**Figure 3.1:** Crab pulsar pulse profiles- The crab pulsar pulse profile was modelled using two Gaussian pulses. The same profile is obtained after epoch folding a set of TOAs (with 0 phase shift) from a simulated photon generator. 27 bins were used for epoch folding and the actual profile.

The crab pulsar was considered to be the source during these simulations. Using the catalogue in [2], the source intensity ($\lambda_s$) is taken as 1.54 $ph/cm^2/s$ and time period ($P$) as 33.4 $ms$. The background radiation ($\lambda_b$) is assumed 0.005 $ph/cm^2/s$, and the detector area is taken as 30 $cm^2$.

To model the pulse profile, the following equation was used: $\lambda(t) = \lambda_b + \lambda_s h(t)$. $h(t)$

is composed of two Gaussian pulses at phase 0.1 and 0.6, with standard deviation 0.01*$P$ and 0.05*$P$ and with heights 1 and 0.5, respectively.

Assuming $T_{obs}$ = 60 s, and $N_b$ = 27. The photon arrival process is simulated for the set period, and we get an empirical profile after epoch folding. Both the empirical and actual profile plots are shown above. In order to have all the profiles lie roughly in the same range, we normalize the profiles so that $\int_0^P \lambda(t)dt = 1$.

## 3.1 Testing the 4 phase estimators

A phase shift of 0.2 is introduced in the rate function, so that now $\lambda'(t) = \lambda(t + 0.2 * P)$ (where P is period of the pulsar signal). To detect this phase shift four estimators are used. They are the Cross Correlation (CC) Estimator, the Fast Fourier Transform (FFT) Estimator, the Maximum Likelyhood Estimator (MLE) and the Non-Linear Least Squares Estimator (NLS).

The plots of phase estimate vs time are shown below. The Estimators are used in the Continuous Processing scheme, without a Kalman Filter.

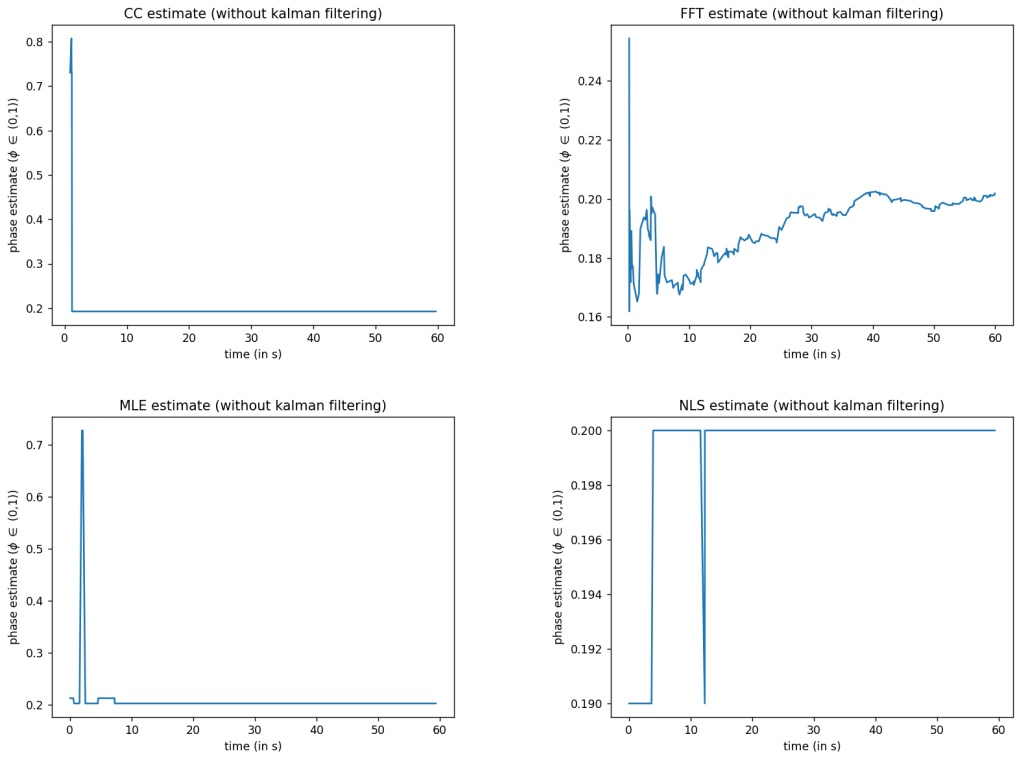


**Figure 3.2:** Phase shift estimate vs time (Crab pulsar)- over the period of 60 seconds new arrivals are accumulated and thus the phase shift estimate improves. But different estimators converge at different rates. Since the crab pulsar has a high source intensity, less time is required to reach the correct estimate.

Kalman filtering is also used with the estimators, and it is observed to smoothen the estimate variation over time.

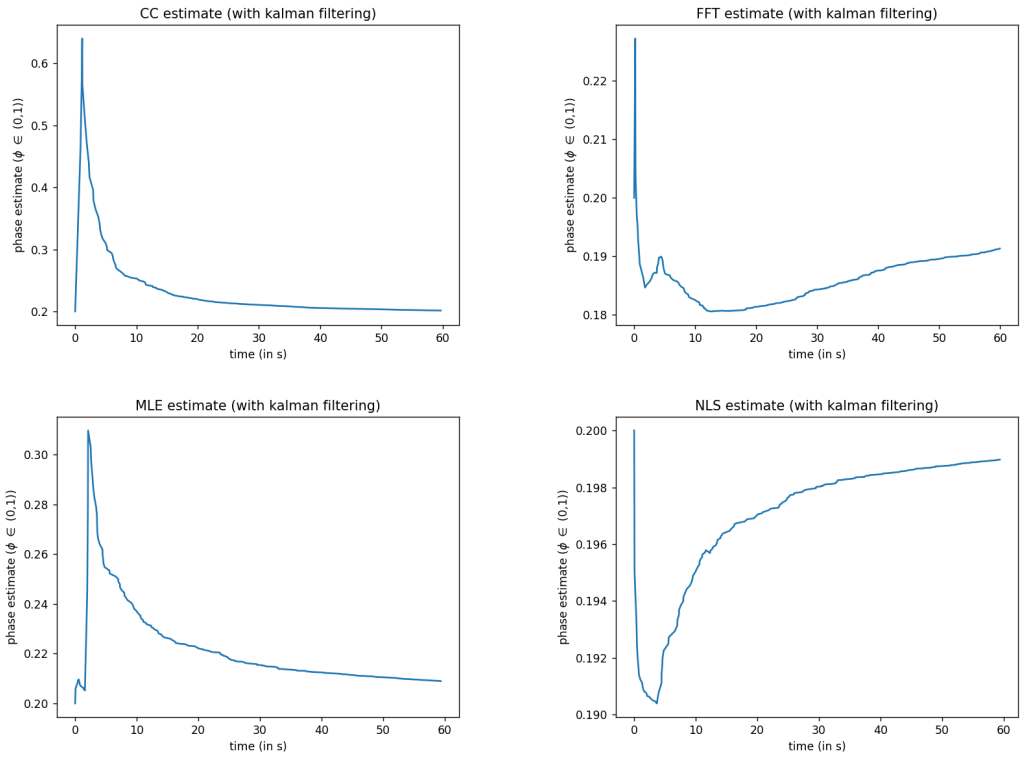


**Figure 3.3:** Kalman filtered phase shift estimates (Crab pulsar)- 1D Kalman filtering was done to remove noise in the estimates. However, this is mainly only useful for the FFT estimator. It also introduces some bias and doesn't let the estimate converge to the actual value for some estimators.

Another pulsar, PSRB 1509 was also modelled and the phase estimation ability of the 4 estimators was also tested. Referring the catalogue in [2], the source intensity and period were taken as $1.62 * 10^{-2}\ ph/cm^2/s$ and $1.5023 * 10^{-1}s$. Due to it's weak nature - an observation period of 500 seconds was taken. The detector area and background radiation are assumed the same.

After performing epoch folding we get the following comparison between the empirical profile and the actual rate function.

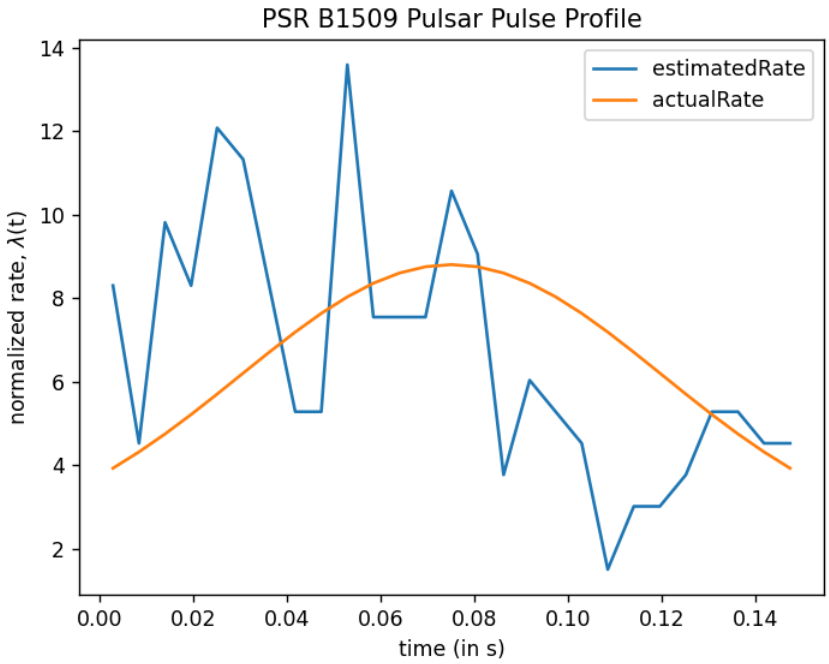


**Figure 3.4:** PSR B1509 pulse profiles- PSR B1509 is a pulsar approximately 17,000 light years away. It has a weaker source intensity (as seen on earth) than crab, and longer rotational period of 150.2 ms. It was modelled as a single Gaussian pulse, and it's epoch folded profile is quite noisy.

The phase estimation plots for this pulsar are shown in figure 3.5.

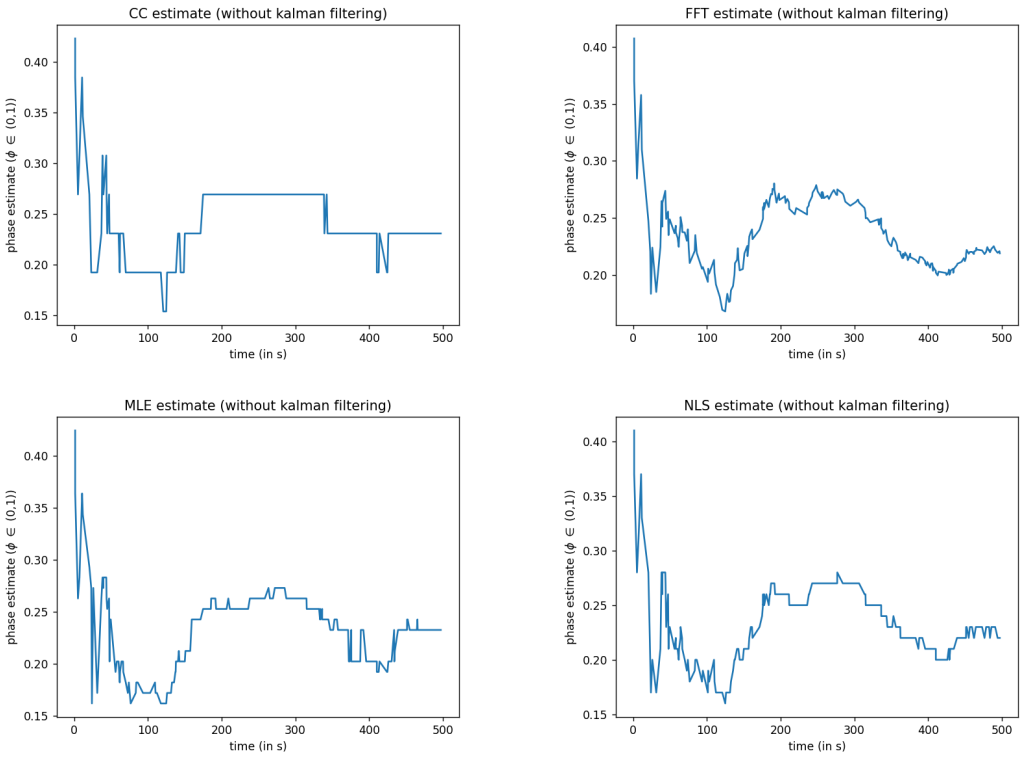


**Figure 3.5:** Phase shift estimate vs time (PSR B1509)- over a period of 500 seconds new arrivals are accumulated and thus the phase shift estimate improves. All the estimators are seen to perform around the same. None of them converge to the correct value within 500 seconds.

The plots after application of kalman filter are shown in figure 3.6.

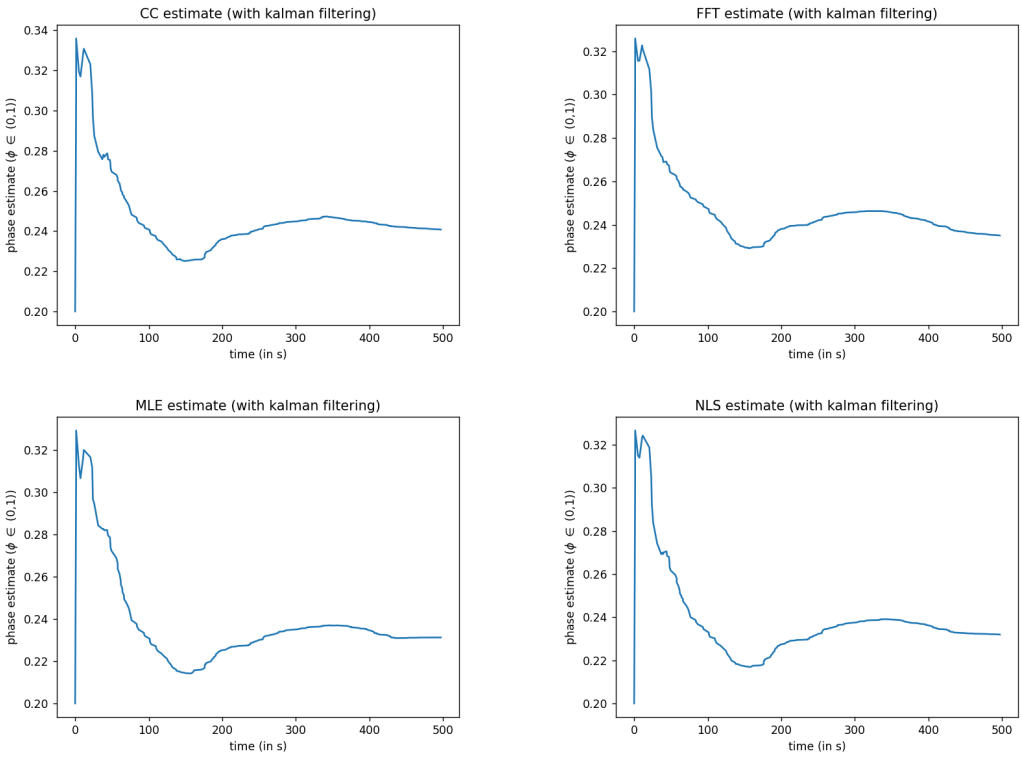


**Figure 3.6:** Kalman filtered phase shift estimates (PSR B1509)- Kalman filtering smoothens the phase estimates, but there is still a significant bias (0.02) compared the correct estimate. This is the case for all the estimators.

Also to check if time period of the pulsar had any effect on the estimation performance - the same simulations were run for the crab pulsar where it's source intensity was assumed the same as PSR B1509 ($1.62 * 10^{-2}\ ph/cm^2/s$) but it's period was it's own ($33.4 * 10^{-3} s$). The observation time was kept the same (500 s). The result of epoch folding is shown below.

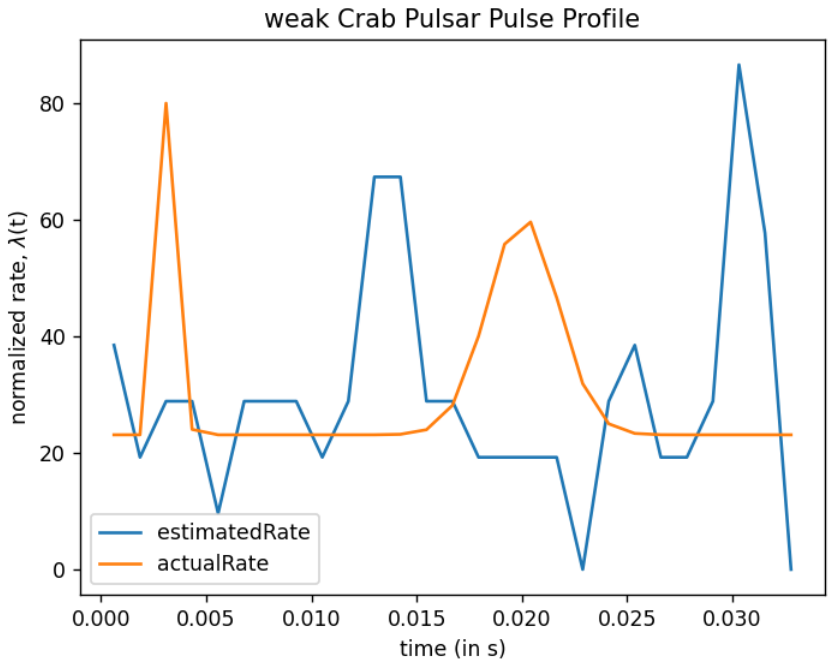


**Figure 3.7:** weak Crab pulsar pulse profiles- The source intensity of the crab pulsar is adjusted to be the same as PSR B1509, and epoch folding is done. Just visually, the obtained profile seems to be less noisy compared to the profile for PSR B1509.

The phase estimation plots for this pulsar are shown in figure 3.8.

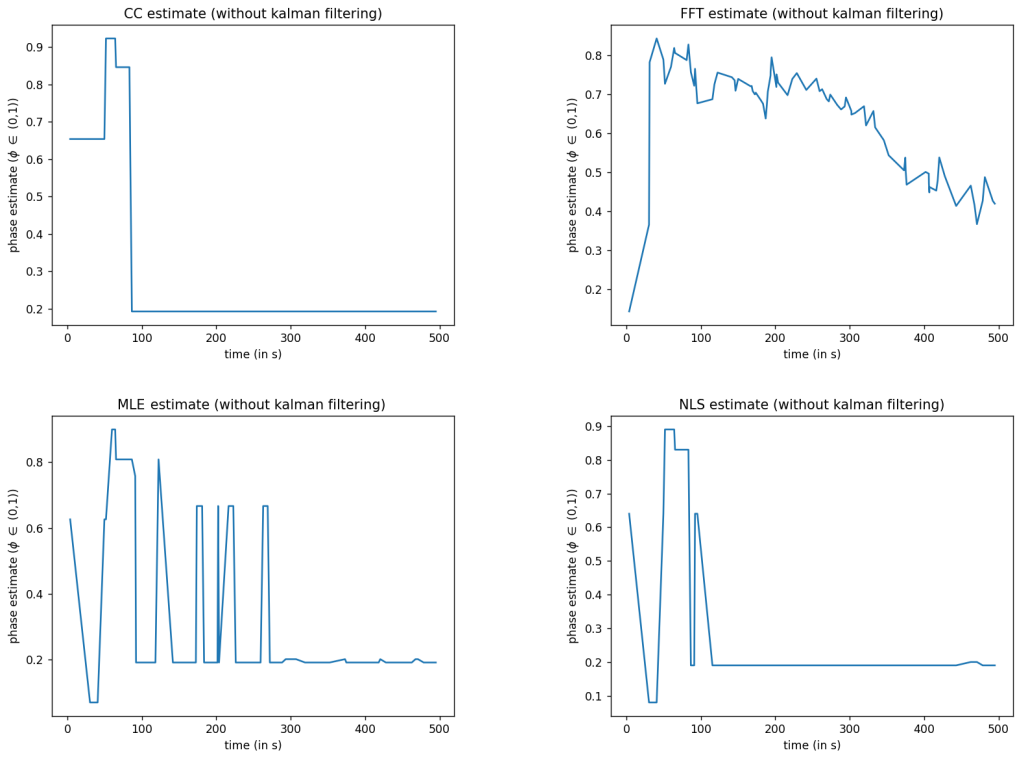


**Figure 3.8:** Phase shift estimate vs time (weak Crab pulsar)- over a period of 500 seconds new arrivals are accumulated and thus the phase shift estimate improves. The order of performance is as follows: CC > NLS > MLE > FFT. The FFT estimator performs especially poorly (0.4 is the final phase estimate instead of the expected 0.2). All other estimators converge to the correct value within atleast 300s.

The plots after application of kalman filter:

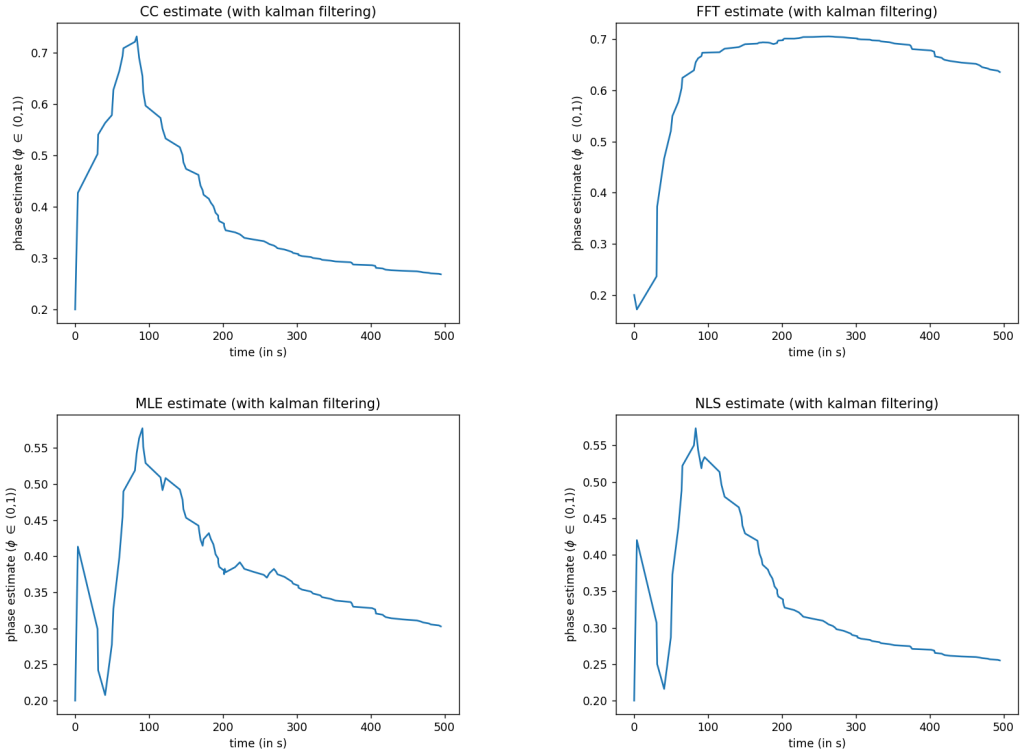


**Figure 3.9:** Kalman filtered phase shift estimates (weak Crab pulsar)- Kalman filtering smoothens the phase estimates. For the FFT estimator, kalman filtering completely ruins the estimation process. For the other three, it introduces a bias of 0.1 in the final phase shift estimate.

## 3.2 Performance of doppler and phase estimators in current scheme

It should be noted that for the doppler estimators, the bias changes based on actual frequency being estimated. However it's magnitude remains roughly of the same order - only sign changes.

**Table 3.1:** Performance of estimators in current scheme

| Estimator | Actual value | Mean | Bias | Variance |
|---|---|---|---|---|
| **Coarse doppler estimator** | 29.94011976 | 29.94010863 | -1.11280e-05 | 7.17879e-08 |
| **CC doppler estimator** | 29.94011976 | 29.94013094 | 1.11885e-05 | 4.44982e-09 |
| **CC phase estimator** | 0 | 0.00625 | 0.00625 | 7.52316e-37 |
| **MLE doppler estimator** | 29.94011976 | 29.94010860 | -1.11574e-05 | 4.77884e-10 |
| **MLE phase estimator** | 0 | 0.00073682 | 0.00073682 | 8.08962784e-07 |

| | |
|---|---|
| a | 6878.137 km |
| Eccentricity | 0.001 |
| Angle of Inclination | 97.8 degrees |
| RAAN | 0.01 degrees |
| Argument of Perigee | 0.01 degrees |
| Initial True Anomaly | 5 degrees |

**Figure 3.10:** orbital parameters

## 3.3 3D orbit simulation

A full 3D orbit simulation was carried out with Poliastro. The orbital parameters chosen are listed in fig 3.10. The simulation is carried out for 5676.978 sec (one full orbit), when testing radial position and velocity estimation.

The estimation of radial position and velocity using the CC and MLE estimators are as shown in figures 3.11 and 3.12.

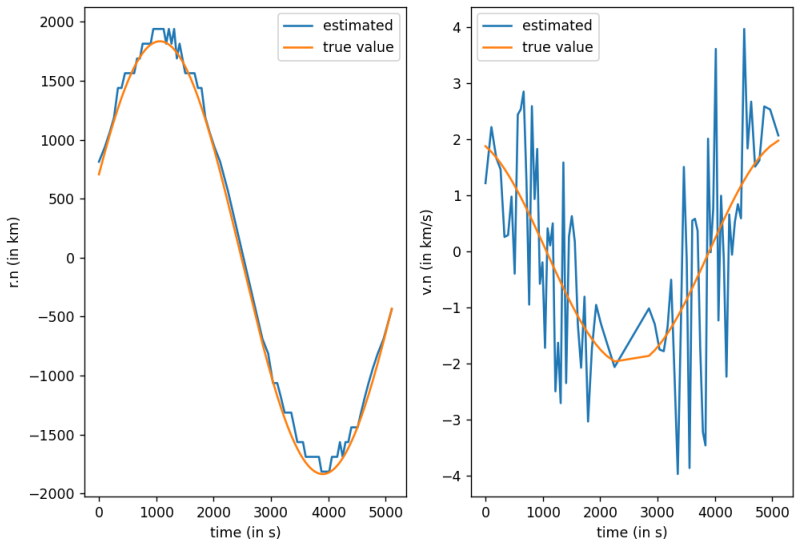


**Figure 3.11:** CC estimator- position and velocity along the line of sight from spacecraft to the Crab pulsar, keeping Geocentre as the reference point. These estimates are calculated from the phase shift and observed frequency estimates given by the CC estimator. Velocity estimates are quite noisy, but position estimates are more stable.

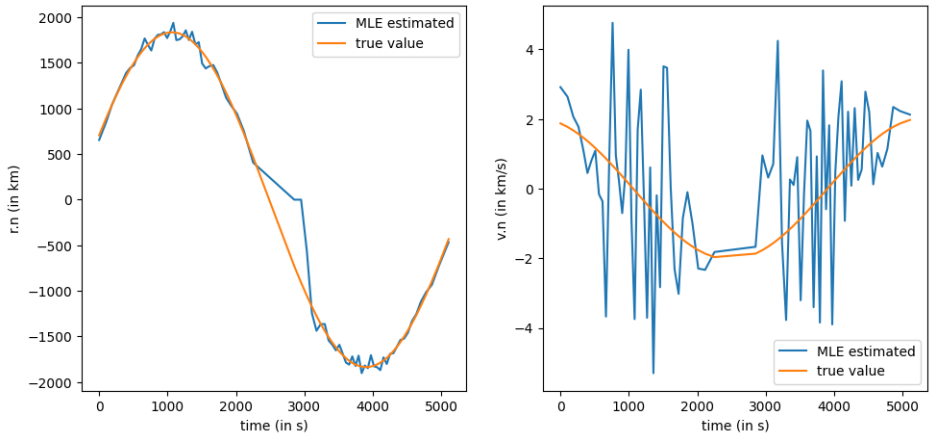


**Figure 3.12:** MLE estimator- The MLE estimator was used to calculate position and velocity along line of sight w.r.t the Crab pulsar. Velocity estimation is noisy and position estimates are stable, similar to the CC estimator. But there is also a large error in the position estimate between 2000s and 3000s of the orbit.

Overall, the CC estimator seems to perform better than the MLE. The MLE has a large error in the position estimation between 2000s and 3000s. This error starts when the phase shift approches zero. The MLE was previously seen to have an issue where the estimate becomes stuck at 0, once phase shift 0 is estimated. To remove this, some code was introduced. This code will have to be investigated to find a solution.

For true anomaly estimation, the cc estimator is used. The true anomaly estimate obtained is quite noisy, and to filter this median filtering was used. The trajectory of the final filtered anomaly estimate, is as shown in figure 3.14. For this estimation, the orbital simulation was only performed for 2000s.

In the figure, there are some periods when the true anomaly estimate suffers large de-

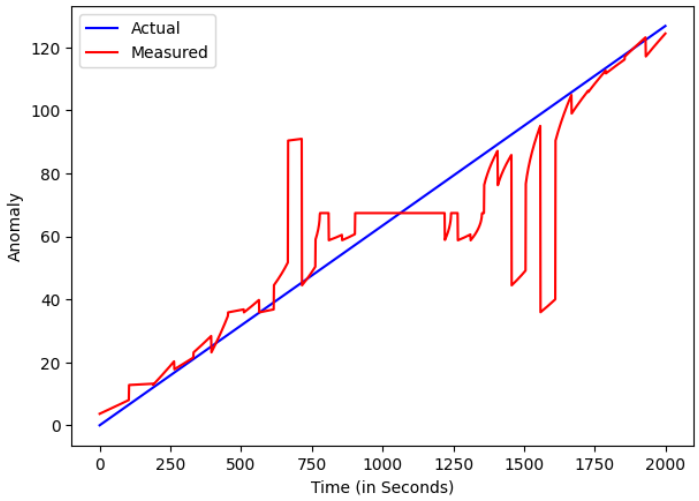


**Figure 3.13:** True anomaly estimated- True anomaly is calculated using the procedure shown in appendix A. True anomaly is an angular parameter describing the position of a body moving along a Keplerian orbit. The noisy peaks are seen due to errors in frequency estimation. Error in estimating the sign of change in frequency is the main cause for this.

viations from the actual true anomaly estimate. This can be attributed to the noisy nature of velocity estimation in the CC estimator.

For true anomaly estimation, it is also necessary to know the direction of radial velocity w.r.t the pulsar [A]. If this direction is incorrectly estimated, the anomaly estimated can be completely different. Since knowledge of direction only depends on correctly estimating

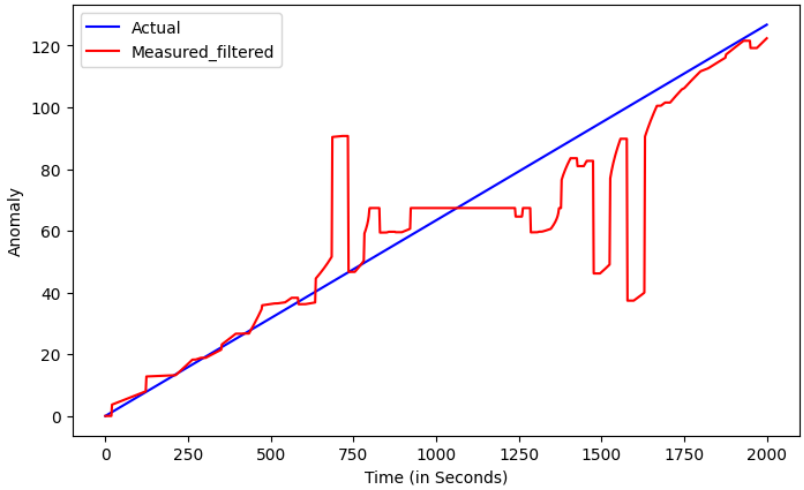


**Figure 3.14:** True anomaly filtered- True anomaly calculated is filtered using median filtering. This removes some of the sharp edges in the estimate, and smoothens the estimate.

the sign of radial velocity, we can use an FIR filter to remove the noise peaks in velocity estimation. The FIR filter used is a low pass filter with a cutoff frequency around 440 mHz. This frequency is 2.5 times the orbital frequency (i.e $f = 1/T_{orbit}$). This FIR filtered estimate of radial velocity is only used to get the direction, and is not used for actual radial velocity estimation. The results of FIR filtering are shown in figures 3.15 to 3.16.

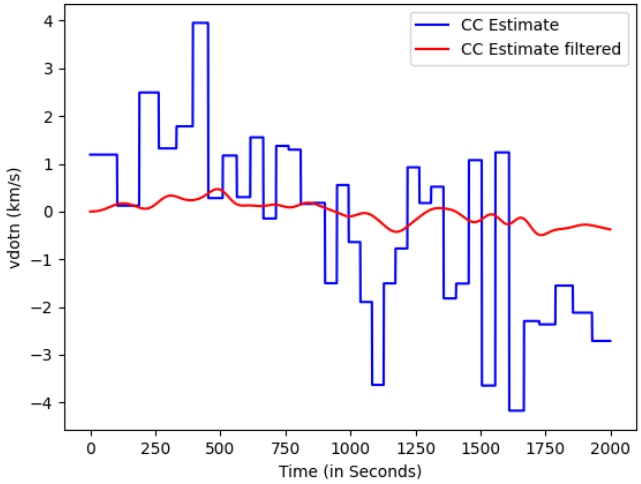


**Figure 3.15:** CC estimate of radial velocity with FIR filtering- There are two plots here, the estimated radial velocity based on the CC estimate of frequency, and the FIR filtered version of the same velocity. The actual radial velocity trajectory is the first half of a sine wave starting at +2km/s and going to -2km/s, as seen in figure 3.11 or 3.12. Although the FIR filtered estimate doesn't contain much information on the magnitude of the velocity, for the most part the sign of the estimate matches that of the actual velocity- and this is what is most important for true anomaly calculation.

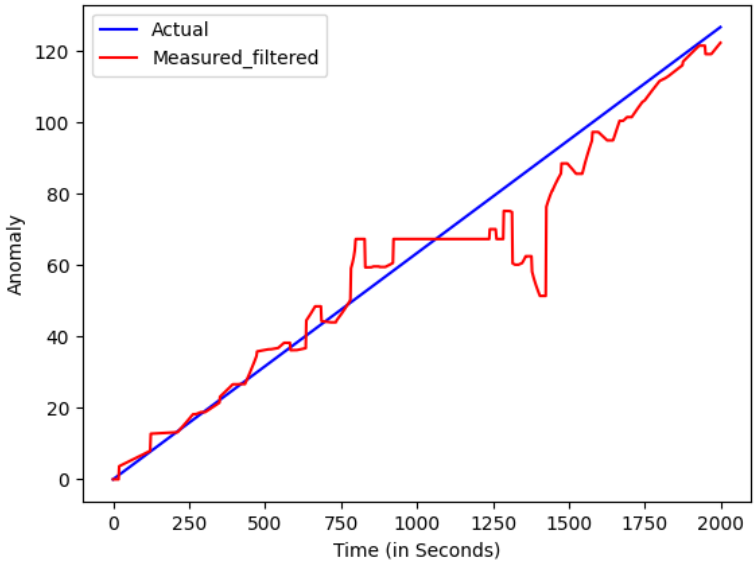


**Figure 3.16:** True anomaly filtered- The FIR filtered velocity estimate is used to calculate true anomaly, and the estimates produced are better than the previous true anomalies calculated. Two large noise peaks are eliminated, and one smaller noise peak is left behind at 1500s.

# Chapter 4
# Conclusion

## 4.1 Summary

This work focused on the estimation algorithms used in the XNav framework. Photon TOA generators were developed which use the method of thinning and phase of arrival concept. All four phase estimators were tested for the continuous time estimation scenario (i.e successive batch estimation using newly recorded photon arrival times- as they arrive), and for that case filtering was done using a 1D kalman filter. The pulsed signal from 2 pulsars was modelled, and signal reconstruction capability using epoch folding was tested for both.

3D orbital simulations were performed, where only single pulsar observations were simulated. Since this is not good enough to perform full state estimation - it is assumed the orbit of the spacecraft is completely known and only it's exact location in that orbit is not known. Using the given orbital parameters, the true anomaly of the spacecraft is estimated.

Regarding epoch folding - it was found that using the average shifted histogram greatly improved the resolution of the folded profile.

## 4.2 Contribution of the work

The major contributions of this ongoing work is listed below:

- This report builds on the estimation algorithms previously developed for the XNav framework. Two additional estimators - coarse frequency estimator and Maximum Likelyhood estimator, have been developed. Velocity estimation capability has been added as well.

- chapter 1 gives a brief overview of the working principle. It also reviews existing research done in the domain of XNav. The main objectives of this work are also mentioned.
- chapter 2 discussing the new algorithms and methods used in this work.
- chapter 3 shows the results from the work done so far. Specifically - phase estimation by the four estimators are compared (for two pulsars), the bias and variance of the estimators are calculated, the CC and MLE estimators are tested in a 3D orbit simulation, and truly anomaly estimation capability is shown.

## 4.3 Future work

The following are a few ideas for further work to be done:

1. *Fuse cc and mle estimates*: Both cc and mle estimates are noisy (especially for velocity estimation). However even with noise, both estimates contain partial information about the true position and velocity. An overall better estimate could be obtained- if these estimates are fused in some way.
2. *3D state estimation*: Modify the algorithms to allow processing of multiple pulsar observations (one at a time), and obtain full 3d position and velocity estimates.
3. *Add the UKF*: Properly integrate the the unscented kalman filter for state estimation. So far adding the UKF did not give much better results.

# Bibliography


[1] S. Shrivastava, "Autonomous spacecraft navigation using x-ray pulsars," Master's thesis, Indian Institute of Technology Kharagpur, 2022.

[2] I. Suneel, "The use of variable celestial x-ray sources for spacecraft navigation," *College Park: University of Maryland*, 2005.

[3] A. Oza, "Navigation in space using x-ray pulsars," 2020.

[4] S. Mishra, "Timing analysis for navigation using x-ray pulsars," 2021.

[5] A. Kandala, A. Oza, B. Saiguhan, S. Mishra, P. Hari, S. Mandal, and H. Simha M S, "Mission concept for demonstrating small-spacecraft true anomaly estimation using millisecond x-ray pulsars," no. SSC21-VI-08, Logan: Utah State University, UT, 2021.

[6] J. Su, H. Fang, W. Bao, H. Sun, L. Shen, and L. Zhao, "Fast simulation of x-ray pulsar signals at a spacecraft," *Acta Astronautica*, vol. 166, pp. 93–103, 2020. [Online]. Available: https://www.sciencedirect.com/science/article/pii/S0094576519313220

[7] L. M. Winternitz, "X-ray pulsar navigation algorithms and testbed for sextant," *2015 IEEE aerospace conference*, 2015.

[8] L. M. B. Winternitz, J. W. Mitchell, M. A. Hassouneh, J. E. Valdez, S. R. Price, S. R. Semper, W. H. Yu, P. S. Ray, K. S. Wood, Z. Arzoumanian, and K. C. Gendreau, "Sextant x-ray pulsar navigation demonstration: Flight system and test results," in *2016 IEEE Aerospace Conference*, 2016, pp. 1–11.

[9] P. S. Ray, K. S. Wood, and M. T. Wolff, "Characterization of pulsar sources for x-ray navigation," 2017.

[10] J. Getchius, A. Long, M. Farahmand, L. Winternitz, M. A. Hassouneh, and J. W. Mitchell, "Predicted performance of an x-ray navigation system for future deep space and lunar missions," Breckenridge, CO, 2019.

[11] P. A. W. Lewis and G. S. Shedler, "Simulation of nonhomogeneous poisson processes by thinning," *Naval Research Logistics Quarterly*, vol. 26, no. 3, pp. 403–413, 1979. [Online]. Available: https://onlinelibrary.wiley.com/doi/abs/10.1002/nav.3800260304

[12] P. Virtanen *et al.*, "SciPy 1.0: Fundamental Algorithms for Scientific Computing in Python," *Nature Methods*, vol. 17, pp. 261–272, 2020.

[13] D. Scott, "Averaged shifted histogram," *Wiley Interdisciplinary Reviews: Computational Statistics*, vol. 2, pp. 160 – 164, 12 2009.

[14] A. A. Emadzadeh and J. L. Speyer, "Navigation in space by x-ray pulsars," *Springer Science  Business Media*, 2011.

[15] T. J. H., "Pulsar timing and relativistic gravity," *Philosophical Transactions of the Royal Society of London. Series A: Physical and Engineering Sciences*, 1992.

[16] N. Ashby and A. R. Golshan, "Minimum uncertainties in position and velocity determination using x-ray photons from millisecond pulsars," *Proceedings of the 2008 National Technical Meeting of The Institute of Navigation*, 2008.

[17] K. D. Anderson, D. J. Pines, and S. I. Sheikh, "Validation of pulsar phase tracking for spacecraft navigation," *Journal of Guidance, Control, and Dynamics*, vol. 38, no. 10, pp. 1885–1897, 2015. [Online]. Available: https://doi.org/10.2514/1.G000789

[18] A. V. Oppenheim, J. R. Buck, and R. W. Schafer, *Discrete-time signal processing*. Prentice Hall, 1999.

[19] S. M. Ross, *Stochastic processes*. Wiley India, 2016.

[20] J. M. Mendel, *Lessons in estimation theory for Signal Processing, communications, and Control*. Prentice Hall PTR, 1995.

# Appendix A

# True Anomaly estimation

True anomaly estimation procedure using time delay measurement is as follows.

$$\vec{r}_{sat,icrf} \cdot \vec{n}_{pulsar,icrf} = c \cdot t_d \tag{A.1}$$

ICRF frame to Orbit Frame transformation:

$$\vec{r}_{sat,icrf} = \vec{r}_{sat,eci} - \vec{r}_{SSB,eci} \tag{A.2}$$

$$\vec{r}_{sat,eci} = Q \cdot \frac{a \cdot (1 - e^2)}{1 + e \cdot cos\theta} \cdot \begin{pmatrix} cos\theta \\ sin\theta \\ 0 \end{pmatrix} \tag{A.3}$$

$$(Q \cdot \frac{a \cdot (1 - e^2)}{1 + e \cdot cos\theta} \cdot \begin{pmatrix} cos\theta \\ sin\theta \\ 0 \end{pmatrix} - \vec{r}_{SSB,eci}) \cdot \vec{n} = c \cdot t_d \tag{A.4}$$

$$\theta = \begin{cases} sin^{-1}\frac{f(t)}{k^2{}_1 + k^2{}_2} - K_2 & \vec{v}_e \cdot \vec{n} > 0 \\ \pi - sin^{-1}\frac{f(t)}{k^2{}_1 + k^2{}_2} - K_2 & \vec{v}_e \cdot \vec{n} < 0 \end{cases}$$

Where,

$$f(t) = \frac{ct_d - \vec{n} \cdot \vec{r}_{SSB,eci}}{a \cdot (1 - e^2)}$$

$$K_2 = sin^{-1}(\frac{k_1}{k^2{}_1 + k^2{}_2})$$

# Analysis and Development of a refined navigation algorithm for XNav mission

ORIGINALITY REPORT

| 8% | 6% | 3% | % |
|---|---|---|---|
| SIMILARITY INDEX | INTERNET SOURCES | PUBLICATIONS | STUDENT PAPERS |

PRIMARY SOURCES

| | | |
|---|---|---|
| 1 | www.coursehero.com<br>Internet Source | 5% |
| 2 | Ping Shuai. "Understanding Pulsars and Space Navigations", Springer Science and Business Media LLC, 2021<br>Publication | 1% |
| 3 | McKee, Paul Dickson. "Autonomous Navigation in Deep Space Using Optical Measurements of Unresolved Planets and Stars", Rensselaer Polytechnic Institute, 2023<br>Publication | <1% |
| 4 | Yidi Wang, Shuangnan Zhang, Minyu Ge, Wei Zheng, Xiaoqian Chen, Shijie Zheng, Fangju Lu. "Fast On-Orbit Pulse Phase Estimation of X-Ray Crab Pulsar for XNAV Flight Experiments", IEEE Transactions on Aerospace and Electronic Systems, 2022<br>Publication | <1% |
| 5 | arxiv.org<br>Internet Source | <1% |

| | | |
|---|---|---|
| 6 | vtechworks.lib.vt.edu<br>Internet Source | <1 % |
| 7 | ebin.pub<br>Internet Source | <1 % |
| 8 | "Position, Navigation, and Timing Technologies in the 21st Century", Wiley, 2020<br>Publication | <1 % |
| 9 | www.diva-portal.org<br>Internet Source | <1 % |
| 10 | Ma, C.-K.. "An inverse method for the estimation of input forces acting on non-linear structural systems", Journal of Sound and Vibration, 20040823<br>Publication | <1 % |
| 11 | Ning, Xiaolin, Mingzhen Gui, Jiancheng Fang, and Gang Liu. "Differential X-ray pulsar aided celestial navigation for Mars exploration", Aerospace Science and Technology, 2017.<br>Publication | <1 % |

| | | | |
|---|---|---|---|
| Exclude quotes | On | Exclude matches | < 10 words |
| Exclude bibliography | On | | |